Composite Structures 210 (2019) 250–261

Contents lists available at ScienceDirect

Composite Structures

journal homepage: www.elsevier.com/locate/compstruct

Single step 3D printing of bioinspired structures via metal reinforced thermoplastic and highly stretchable elastomer

Armita Hamidi, Yonas Tadesse*

Humanoid, Biorobotics and Smart Systems (HBS) Laboratory, Department of Mechanical Engineering, The University of Texas at Dallas, Richardson, TX 75080, United States

ARTICLE INFO

Keywords:
Additive manufacturing
Continuous metal fiber reinforced
Very soft elastomer
Bioinspired 3D printed joint

ABSTRACT

Multimaterial additive manufacturing technique is a great alternative approach for fabrication of complex structures with diverse mechanical properties compared to traditional assembly process. Fused deposition modeling is a simple, popular and affordable technique, which is available in numerous desktop 3D printers nowadays. However, this technology is not developed considerably to co-fabricate highly stretchable (800% strain) elastomer materials with low stiffness and high strength parts in one single build platform. In this paper, a single step fabrication of a novel bioinspired joint system, consisting of dissimilar materials with high strength and high strain elements is developed by an inexpensive 3D printer. The joint consists of continuous metal fibers reinforced thermoplastic part that resembles bones and soft elastomer that mimics soft tissues. Tensile test results of the 3D printed reinforced thermoplastic part showed a 78% increase in strength, which can be competed with natural bone. Highly stretchable elastomer is used for the soft parts that was directly 3D printed and simultaneously cured by heating. Overall, a simple and cost effective heterogeneous material manufacturing technique is developed that maintained high mechanical strength and sufficient elasticity, to produce a bioinspired joint that composed of a rigid skeleton covered by a very soft elastomer.

1. Introduction

Fused deposition modeling (FDM) is a 3D printing method in which successive layers of molten thermoplastic are placed on top of each other by moving an extruder through x, y and z stages. However, delamination of the layers affects the material behavior and the dimensional accuracy of the final product [1,2]. Moreover, limited number of materials, namely thermoplastics and composites, are currently used in this technology because of their suitability [3]. Due to the mentioned constraints, FDM is mainly used for manufacturing parts such as conceptual models, testing prototypes or low volume end-products, but improving the technology, will pave the way for the realization of a wide range of applications such as aerospace, automotive, robotics and medical equipment [4]. In this regard, nanocomposites, short fiber reinforced filaments and continuous fiber 3D printing are employed to improve mechanical properties of thermoplastic 3D printed parts as shown in Fig. 1 [5–9].

Several studies showed that nanocomposites are essential for 3D printing for sensors [10,11], batteries [12] and electrical wiring of robots [13,14] (Fig. 1(a) & (b)). There are also numerous studies in the area of short fiber reinforced thermoplastics [7,15,16]. Tekinalp et al. [15] showed that fiber length, fiber orientation, and porosity affect the mechanical properties of composites. However, the average fiber length after extruding decreased with increasing fiber loading in short fiber reinforced composites regardless of the initial fiber length because of the significant fiber breakage.

Continuous fiber reinforced polymer manufacturing is another technique that enhances mechanical properties of 3D printed parts. The fibers can be placed into the printing filaments prior to the nozzle (Fig. 1(c1)) or after the extrusion (Fig. 1(c2)&(c3)) [8]. Mori et al. [17] showed that continuous carbon fibers have a great influence on the strength of FDM products. In their first study, carbon fibers were sandwiched by lower and upper 3D printed plastic plates and heated to bond (Fig. 1(c3)), which increased tensile strength and strain. In their second study, the carbon fiber was inserted in a 3D printer extruder before an acrylic butadiene styrene (ABS) filament passed through the drive gears. The tensile force and the elongation increased noticeably compared to both the 3D printed specimen without any fibers and the first sample. Namiki et al. [18] used polylactic acid (PLA) filament and a carbon fiber bundle in a 3D printer for continuous fiber reinforcement. The PLA filament and the carbon fiber brought together in the heater while PLA was heated and melted in, and carbon fiber was

* Corresponding author.
E-mail address: yonas.tadesse@utdallas.edu (Y. Tadesse).

https://doi.org/10.1016/j.compstruct.2018.11.019
Received 30 March 2018; Received in revised form 2 November 2018; Accepted 6 November 2018
Available online 13 November 2018
0263-8223/

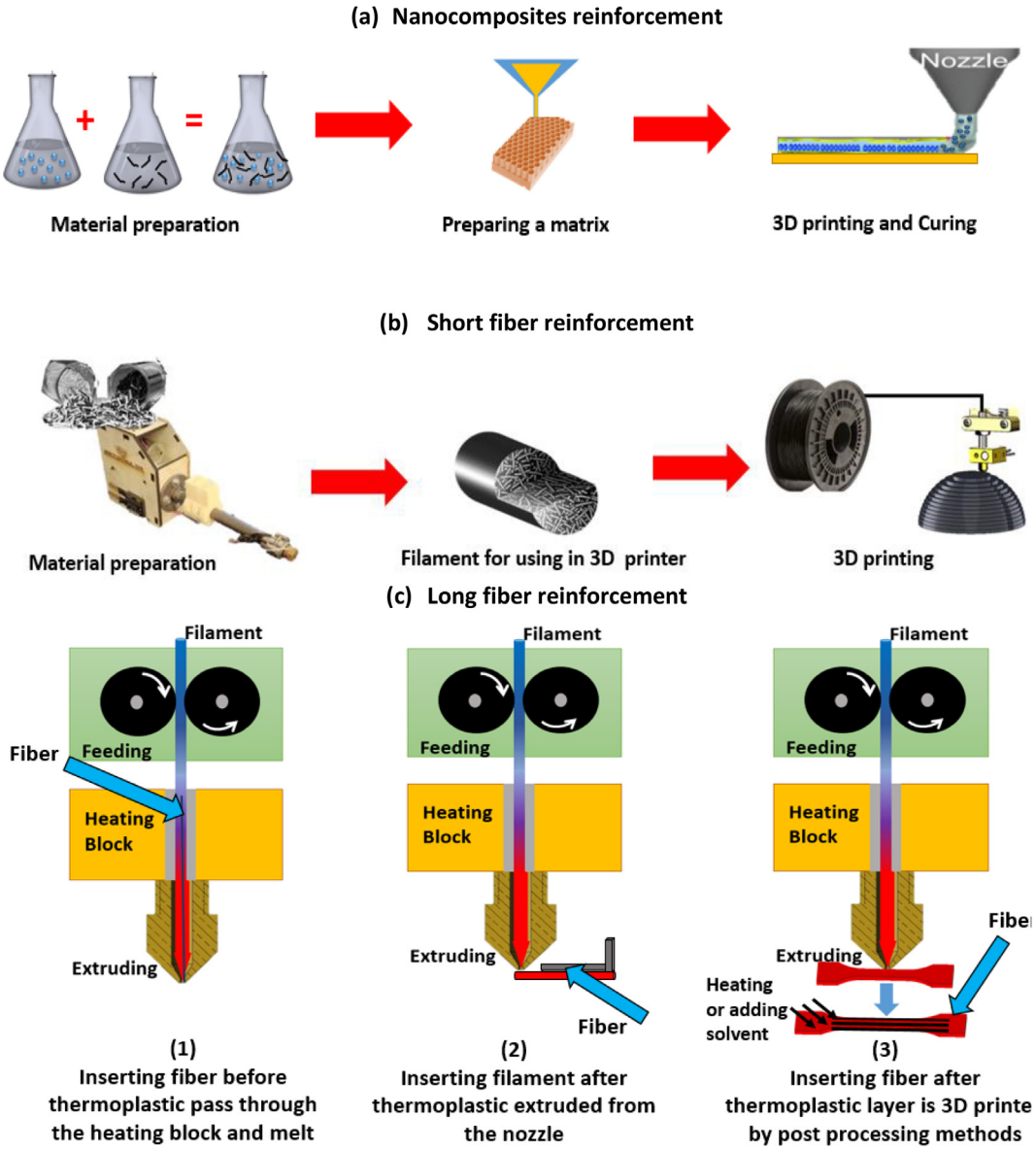

Fig. 1. Schematic diagram of 3D printing reinforcement methods: (a) Nanocomposites reinforcement (used widely with inkjet 3D printing), (b) short fiber reinforcement (used with FDM 3D printing), and (c) long fiber reinforcement [5–16].

impregnated into it (Fig. 1(c1)). The strength of the carbon fiber reinforced thermoplastic specimen reached to 90 MPa by this method. In order to achieve better bonding between the fiber and the thermoplastic matrix, Li et al. [19] tested different 3D printed samples with carbon fiber reinforced PLA and modified carbon fiber reinforced PLA. The modified carbon fibers were produced by infiltration of row carbon fiber in an aqueous solution of DCM (dichloromethane), PLA and antifoaming agents to improve the interfacial strength and bonding between PLA layers. They obtained improved tensile strength and flexural strength for the reinforced composites with surface modified carbon fiber, which were 13.8% and 164% higher than the original carbon fiber reinforced samples. There are several more studies on mechanical properties enhancement by continuous fiber 3D printing from year 2014 to 2018 [1,20–29], which we presented the summary in Fig. 2.

Among commercial 3D printers, MarkOne is one of the first desktop 3D printers, which is released for fabricating continuous fiber reinforced 3D printed composites. Melenka et al. [26] studied the dimensional accuracy, ultimate tensile strength and elastic modulus of this 3D printer (MarkOne) using Kevlar fiber reinforced samples. They also examined the effect of fiber reinforcement and developed a predictive model based on a volume averaging stiffness method in order to predict the tensile properties of the composite. However, their method was not accurate for fiber volume fractions less than 8%. In their model, the theoretically predicted elastic modulus of reinforced parts with 2, 4 and 5 concentric Kevlar rings were different from experimental results. They mentioned that this difference could be due to the waviness and misalignment of the Kevlar fibers and the poor bonding between the fibers and the nylon matrix.

3D printing technology can also reduce the current manufacturing challenges in the production of multifunctional materials [30]. For instance, Mansouri et al. [31] investigated the mechanical response of a co-continuous multimaterial composites (Bayblend™/TPU) manufactured by the FDM method through experiments and simulations. TPU is a soft thermoplastic polyurethane and Bayblend™ is a blend of ABS and Polycarbonate (PC). They demonstrated that embedding of the soft phase (TPU) into the hard cellular structure (Bayblend) allows it to deform more elastically, which provides more flexibility to the whole composite and a strain recovery between 82% and 93%. Elastomers are ideal materials for fabricating soft robots and actuators due to their excellent elasticity and resilience [32,33]. However, the curing process

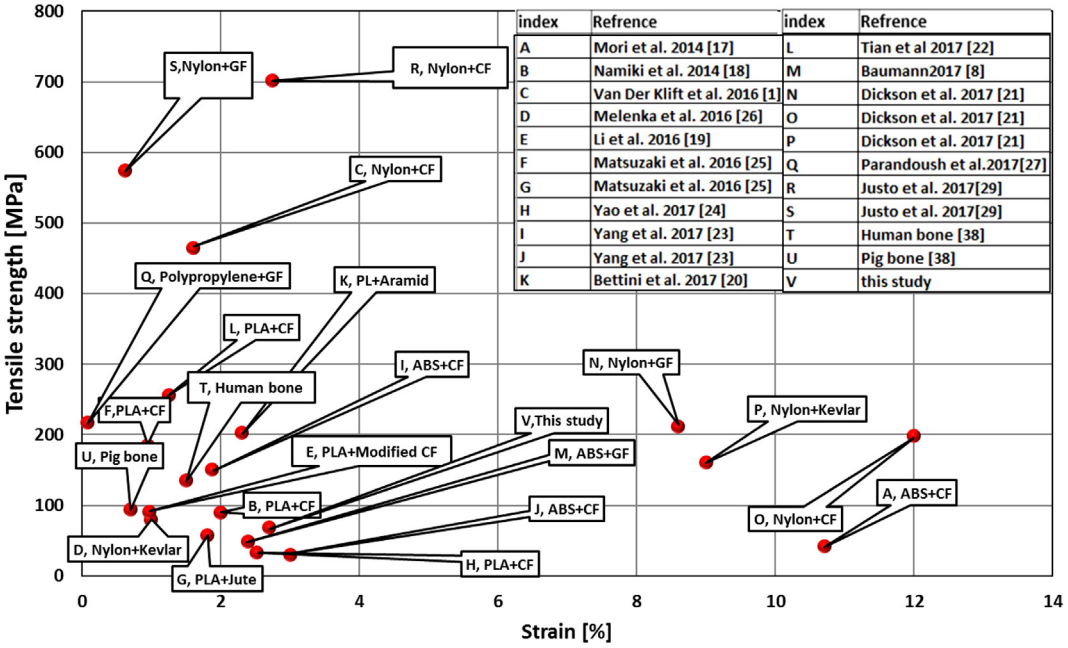

Fig. 2. Comparison of 3D printing continuous fiber reinforcement studies until 2018.

of the elastomer (namely silicone rubber) in these applications limits the fabrication to strictly follow the traditional methods such as molding and casting. Recently, a few methods for 3D printing silicone rubbers have been developed, which are mostly based on the direct ink writing [34,35]. In these methods, custom made materials, which take few hours for preparing and curing process are commonly used. Patel et al. [36] reported 3D printing soft actuators and bucky ball electronic switches with highly stretchable and UV curable elastomer by digital light processing 3D printing technique. They claimed that the elastomer can stretched up to 1100%. Currently, polyjet is the most commonly used 3D printing technology for combining different materials with relatively large difference in their mechanical properties in the same part. This technology is expensive and have limited yield strains. For example, the most advanced 3D printer, Connex from Stratasys Ltd. can fabricate a soft material with shore hardness of 27A (soft as a rubber), which is very hard compared to the soft elastomer presented in this work.

The primary aim of this study was to create a high strength 3D printed bone-like structure for use in a bioinspired joint design. The joint design was proposed by Tadesse et al. [37] and consists of a ball and socket joint with elastic capsules, soft polymer actuators (twisted and coiled polymer muscles), and soft silicone support around the joint. In order to avoid tedious and time consuming aspects of the fabrication process for adding elastomer to the joint, a custom made 3D printer set up was developed for effective fabrication of the elastomer as well as other hard structural parts that serve as skeleton.

Over all, this paper provides a solution for a single-step manufacturing of a bioinspired joint consisting of both high strength materials and soft materials. The high strength material is reinforced thermoplastic (e.g PLA) part, and it resembles the skeleton of human bone while the elastomer part mimics the soft tissues. A real bone structure in human and pig has a tensile strength of 120–150 MPa and 88–100 MPa and a strain to failure of 1.5% and 0.7%, respectively [38]. In this work, we have attempted to increase the strength of the sample with continuous fiber technique to get the mechanical properties similar to the bone structure. After 3D printing the reinforced structure, highly stretchable elastomer was 3D printed on top of it and forming a bioinspired joint.

The rest of the paper is organized as follows. Section 2 will discuss about the materials and experimental setups. Section 3 will be dedicated for modeling and simulation of the composite structure using existing models. Section 4 illustrates experimental results and Section 5 describes the bioinspired joint fabrication and characterization. Finally, the summary and conclusions are presented.

2. Materials and methods

2.1. Materials

In this study, five different materials were investigated. *Sample1*: PLA and copper wire, *sample 2*: PLA and steel wire, *sample 3*: PETG/carbon nanotubes (3DXNano™ ESD) and copper wire, *sample 4*: PETG/carbon nanotubes (3DXNano™ ESD) wire and *sample 5*: pure silicone elastomer. We also studied a metal reinforced polymer along with a highly stretchable elastomer for bioinspired joint fabrication. For this purpose, bright finish conductive copper wire, with diameter of 0.127 mm and spring-Back 302/304 stainless steel wire with diameter of 0.1778 mm, were used as reinforcement metal fibers along with 1.75 mm diameter PLA filament as the polymer matrix. For comparison purposes and better bonding, PETG/carbon nanotubes (3DXNano™ ESD) filament with diameter of 1.75 mm, was also used along with the steel wire for 3D printing samples. This filament consists of polyethylene terephthalate glycol copolymer (PETG), which has a higher density (1.38 g/cm^3) than PLA and it is also reinforced by multi-walled carbon nanotubes (MWCNTs). This filament has a lower tensile strength (46 MPa) compared to PLA, but the elongation is improved. The tensile strength, modulus and diameter of the materials are shown in Table 1. To fabricate the soft parts of the bioinspired joint with high deformation, a platinum-catalyzed silicone Ecoflex 00-30 (Smooth-On, Inc) was used. The elastomer was prepared by mixing Ecoflex rubbers A and B, 1:1 by volume and 20% (volume fraction). Silicone thinner (Smooth-On, Inc.) was also added to the mixture to lower the viscosity and increase the pot life of the elastomer.

2.2. 3D printer set up

The printer used in this work was an assembled MakerFarm Prusa 8″ i3v Kit controlled with RAMBo1.3 (Ultimachine) mother board. Open source 3D printer control software, Repetier-Host was used for controlling the 3D printing process. The printing bed had a heating plate

Table 1
Technical properties of the filaments and fibers.

PLA filament	Tensile strength (σ_{up})	57.8 MPa
	Tensile Modulus (E_p)	3.5 GPa
	Diameter (r_p)	1.75 mm
	Shear modulus (G_p)	2.4 GPa
	Poisson's ratio (ν_p)	0.366
PETG + CNT filament*	Tensile strength (σ_{upe})	46 MPa
	Tensile Modulus (E_{pe})	1.794 GPa
	Diameter (r_{pe})	1.75 mm
	Shear modulus (G_{pe})	0.655 GPa
	Poisson's ratio (ν_{pe})	0.37
Steel wire **	Tensile strength (σ_{us})	1413.5 MPa
	Tensile Modulus (E_s)	193 GPa
	Diameter (r_s)	0.1778 mm
	Shear modulus (G_s)	75
	Poisson's ratio (ν_s)	0.333
Copper wire***	Tensile strength (σ_{uc})	200 MPa
	Tensile Modulus (E_c)	117 GPa
	Diameter (r_c)	0.127 mm
	Shear modulus (G_c)	45 GPa
	Poisson's ratio (ν_c)	0.355

*3DXNano™ ESD PETG + Carbon Nanotube Filament Product Data Sheet available at www.3DXTech.com.
**Spring-Back 302/304 Stainless Steel Wire #9495K112 MacMaster-CARR.
***Mirror-Like Multipurpose 110 Copper Wire MacMaster-CARR.

and a glass on the top. All the fiber reinforced thermoplastic parts were 3D printed with one nozzle of size 0.8 mm diameter (brass material). For 3D printing the elastomer material, a simple paste extruder, Discov3ry Complete (Structur3D Printing, Canada) was adopted to the set up. The paste extruder was consisted of 60 cc syringe, 0.6 m long plastic tube with inner diameter of 3.17 mm and a plastic cone tip nozzle with diameter of 0.7 mm. The material in the syringe is pushed throw the tube by the force that a motor applies to a rod, which is connected to the syringe plunger.

2.3. Preparing specimen for tensile test and 3D printing

Plastic reinforced samples: For sample preparation, the thermoplastic filament was inserted from the top of the extruder while the metal fiber was guided to the extruder after the filament driving gears right at the nozzle inlet (Fig. 3(a)). It is observed that inserting the fiber along with the thermoplastic filament at the same place, causes the fiber extruded with different speed than the thermoplastic filament and therefore, the extruded plastic curls up or the fiber stretches and breaks. Two different patterns, namely rectilinear and concentric infill patterns were chosen to print the specimen (Fig. 3(b) & (c)) to observe the effect of the fiber direction on the mechanical properties of the specimen. The thickness of the ASTM D638-14 Type 1 standard sample for tensile test is 3.2 mm. Our single 3D printed layer thickness was measured as 0.8 mm. Therefore, each specimen was sliced into only 4 vertical layers, in which a maximum of 2 of them could be applied for reinforcement. The first layer of all samples were 3D printed with pure thermoplastic layer, which provided a better surface for sticking the fiber on and a persistent traction force to pull the fiber cladded out of the nozzle. The last layer was also 3D printed with pure thermoplastic to preserve the surface quality of the samples. Finally, prior to performing the tensile test, the 3D printed samples were measured to evaluate the dimensional accuracy of the 3D printer and calculate the exact cross section area of each sample. The highest dimensional error was occurred in the 3D printed PETG samples with steel fibers. In this sample, the delamination of the layers due to the inserted steel wires results in increase in thickness of the sample by 0.8 mm from the standard design. All other 3D printed samples were fabricated with dimensional error (along length, width and thickness) less than 0.5 mm, due to the size of the nozzle used for the experiment.

Silicone elastomer samples, casted and 3D printed: The casted elastomer samples were prepared by molding it in a 3D printed dog bone mold that was designed based on ASTM D412 Type C with the thickness of 4 mm after it cured. These samples were cured for 4 h at the room temperature and the elastic properties of them were investigated. The effective cross sectional areas of the samples were 33 mm by 6 mm middle rectangular shape.

For 3D printing the same elastomer part, the uncured elastomer was poured to the syringe after preparing the material as mentioned in Section 2.1. The 3D printed bed is heated to 100 °C for increasing the curing time of the sample. All the 3D printed silicone samples had a dimensional error less than 0.2 mm (measured with calipers). The reason for less error is the compact nature of uncured silicone layer applied one over the other and the smaller nozzle size as well as the absence of wires in the samples. The printer set up parameters for elastomer, metal reinforced PLA and metal reinforced PETG + CNT

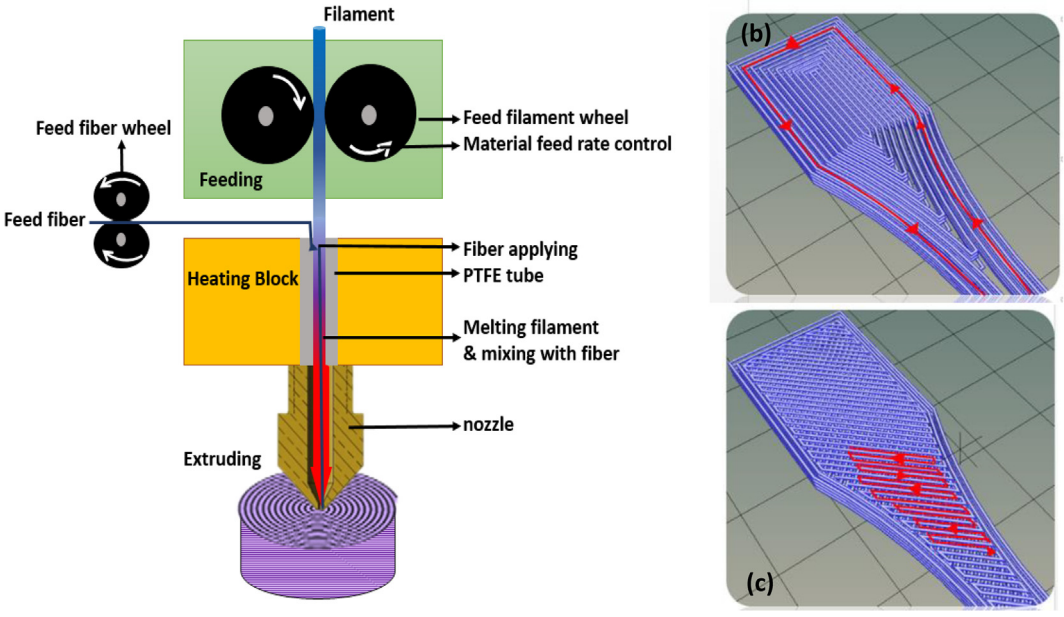

Fig. 3. (a) 3D printer extruder schematic set up, (b) fiber printing direction with concentric infill and (c) fiber printing direction with rectilinear infill pattern.

Table 2
3D printing experimental parameters.

PLA Fiber Reinforced		PETG + CNT Fiber Reinforced		3D Printed Ecoflex 0030	
Nozzle Diameter	0.8 mm	Nozzle Diameter	0.8 mm	Nozzle Diameter	0.5 mm
Layer Thickness with fiber	1.61 mm	Layer Thickness with fiber	1.61 mm	Layer Thickness after curing	0.7 mm
Nozzle Temperature	205 °C	Nozzle Temperature	230 °C	Nozzle Temperature	25 °C (room temperature)
Print Bed Temperature	70 °C	Print Bed Temperature	75 °C	Print Bed Temperature	100 °C
Head translation speed for first layer	10 mm/s	Head translation speed for first layer	10 mm/s	Head translation speed for first layer	15 mm/s
Head Translation Speed for all layers (except first layer)	5 mm/s	Head Translation Speed for all layers (except first layer)	5 mm/s	Head Translation Speed for all layers (except first layer)	15 mm/s
Layer height	0.8 mm	Layer height	0.8 mm	Layer height	0.43 mm
Infill density	100%	Infill density	100%	Infill density	100%

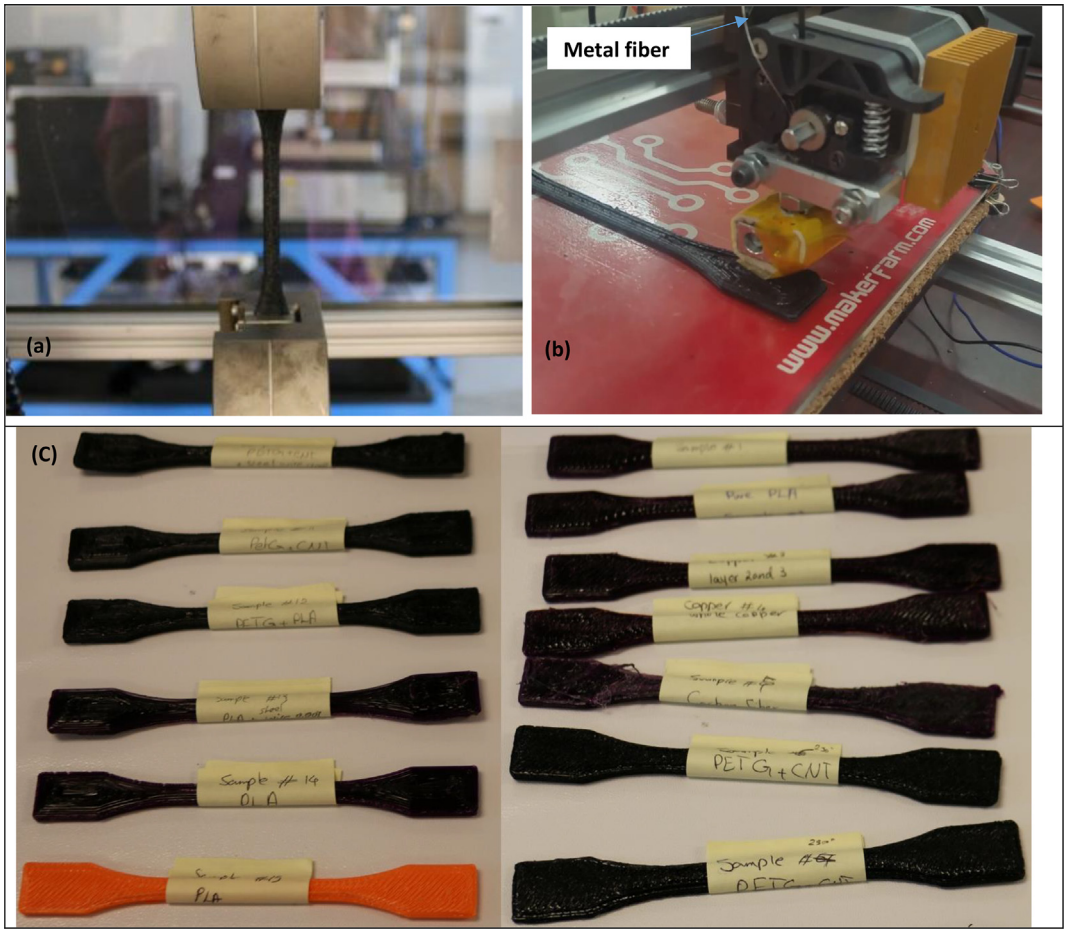

Fig. 4. (a) Tensile test with Instron Universal tensile system, (b) 3D printing metal fiber reinforced samples for tensile test and (c) all test specimen prepared for tensile test.

were described in Table 2. Tensile tests were done for all plastic reinforced and elastomer specimen on Instron Universal Tensile system (Fig. 4(a)) at rates of 5 and 500 mm per min, respectively. Fig. 4(b) shows the metal fiber /thermoplastic printing and the printer head setup. Fig. 4(c) shows all the continuous metal fiber reinforced samples prepared for tensile test.

3. Modelling

In this section, three mathematical models were used to predict the mechanical properties of fiber reinforced thermoplastics. We used the existing models, rule of mixture, The Halpin-Tsai and classical laminate plate theory for evaluation only [36–41]. These models, are derived base on the properties of the individual components of the composite. The following assumptions were made for the current study: (1) the fibers are circular in geometry, (2) the host matrix (PLA or PETG) and fiber reinforcement have equal strain at failure and (3) the tensile tests are done in the direction of fiber and compared with the 3D printed samples by concentric pattern.

3.1. Rule of mixture (ROM)

Rule of mixture is a simple method that can be used to predict the elastic properties of a composite in the direction of the fibers [39]. According to this models, Young's modulus and tensile strength are calculated using the following equations:

$$E_c = V_f E_f + V_m E_m \quad (1)$$

where the E_c, E_f, E_m are elastic modulus of the composite, fiber and matrix, respectively. V_f and V_m denotes the fiber and the matrix volume

ratios, respectively.

3.2. The Halpin—Tsai model

This model is widely used for predicting the elastic properties of short fiber reinforced the rmoplastics and tensile modulus [40]. Eq. (2) is used to predict the tensile modulus and strength of composites in Halpin_Tsai model [41]:

$$E_c = E_m \left(\frac{1 + 2\left(\frac{l}{D}\right)\left(\frac{E_f / E_m - 1}{E_f / E_m + 2\left(\frac{l}{D}\right)}\right) V_f}{1 - \left(\frac{E_f / E_m - 1}{E_f / E_m + 2\left(\frac{l}{D}\right)}\right) V_f} \right) \tag{2}$$

All parameters are as defined before, l is the length of the fiber in one-direction and D is the diameter of the fiber.

3.3. Classical laminate plate theory (CLPT)

CLPT is another method that can be applied for characterizing FDM 3D printed part including continuous fibers and voids [26,42–44]. For this model, each 3D-printed layer is considered as a lamina (Fig. 5). Then the elastic modulus of the lamina is calculated using area weighted method by following equation:

$$E = \frac{A_f E_f + A_m E_m}{A_{total}} \tag{3}$$

where the E, E_f and E_m are elastic modulus of the composite lamina, fiber and matrix, respectively. A_t, A_f and A_m denotes the total, fiber and matrix cross sections:

$$A_f = n_f \pi r^2, \quad A_t = n_l \pi R_1 R_2 \quad \text{and} \quad A_m = A_t - A_f \tag{4}$$

where n_f and n_l are the average number of fibers and layers rested in one lamina, r is the fiber radius, R_1 and R_2 are the radii of the elliptical cross section of the layer.

The stiffness matrix of each lamina in CLPT for laminated plates consisting of multiple unidirectional laminae are given as:

$$\begin{bmatrix} \sigma_{11} \\ \sigma_{22} \\ \sigma_{12} \end{bmatrix} = \begin{bmatrix} \frac{E_{11}}{1-\nu_{12}\nu_{21}} & \frac{E_{11}\nu_{21}}{1-\nu_{12}\nu_{21}} & 0 \\ \frac{E_{11}\nu_{21}}{1-\nu_{21}} & \frac{E_{22}}{1-\nu_{12}\nu_{21}} & 0 \\ 0 & 0 & G_{12} \end{bmatrix} \begin{bmatrix} \varepsilon_{11} \\ \varepsilon_{22} \\ \varepsilon_{12} \end{bmatrix} \tag{5}$$

where σ_{ij} and ε_{ij} are in-plane stress and strain, respectively. E_{11} and E_{22} represent the longitudinal and transverse elastic modulus of the layers, G_{12} represents the in-plane shear modulus and ν_{12} and ν_{21} are the major and minor Poisson's ratio. The 3×3 matrix is the stiffness matrix. The porosity ρ is directly included in the material properties as:

$$E_{11} = (1 - \rho)E \tag{6}$$

$$E_{22} = (1 - \rho^{0.5})E \tag{7}$$

$$G_{12} = G\frac{(1-\rho)(1-\rho^{0.5})}{(1-\rho) + (1-\rho^{0.5})} \tag{8}$$

$$\nu_{12} = (1 - \rho)\nu \tag{9}$$

$$\nu_{21} = (1 - \rho^{0.5})\nu \tag{10}$$

In Eqs. (6)–(10), ν is the Poisson's ratio obtained from the material and E is elastic modulus of each lamina, which is calculated from Eq. (3). The stiffness matrix is defined as:

$$[Q] = \begin{bmatrix} \frac{E_{11}}{1-\nu_{12}\nu_{21}} & \frac{E_{11}\nu_{21}}{1-\nu_{12}\nu_{21}} & 0 \\ \frac{E_{11}\nu_{21}}{1-\nu_{21}} & \frac{E_{22}}{1-\nu_{12}\nu_{21}} & 0 \\ 0 & 0 & G_{12} \end{bmatrix} \tag{11}$$

The general orthotropic lamina [39] assumption is used in this case, since the fiber and matrix orientation are in the same direction with angle of 0°. Then the laminate extensional (A), coupling (B) and bending (D) stiffness matrices can be obtained by Eqs. (12)–(14):

$$A = \sum_{k=1}^{n} ([Q])(z_k - z_{k-1}) \tag{12}$$

$$B = \frac{1}{2}\sum_{k=1}^{n} ([Q])(z_k^2 - z_{k-1}^2) \tag{13}$$

$$D = \frac{1}{3}\sum_{k=1}^{n} ([Q])(z_k^3 - z_{k-1}^3) \tag{14}$$

where z_k represents the vertical position in the lamina from mid-plane. By cascading A, B and D matrices, we obtain a 6×6 matrix [C]:

$$[C] = \begin{bmatrix} A & B \\ B & D \end{bmatrix} \tag{15}$$

In the case of uniaxial tensile loading, the load is applied in x-direction only. Thus, the mid-plane young's modulus along x for a laminate with thickness of t (per unit width) can be determined by Eq. (16):

$$E_{xx} = \frac{1}{(t)[C]_{11}^{-1}} \tag{16}$$

Eq. (16) is used to compare the elastic modulus of 3D printed samples with different fiber materials, which will be discussed in the next section.

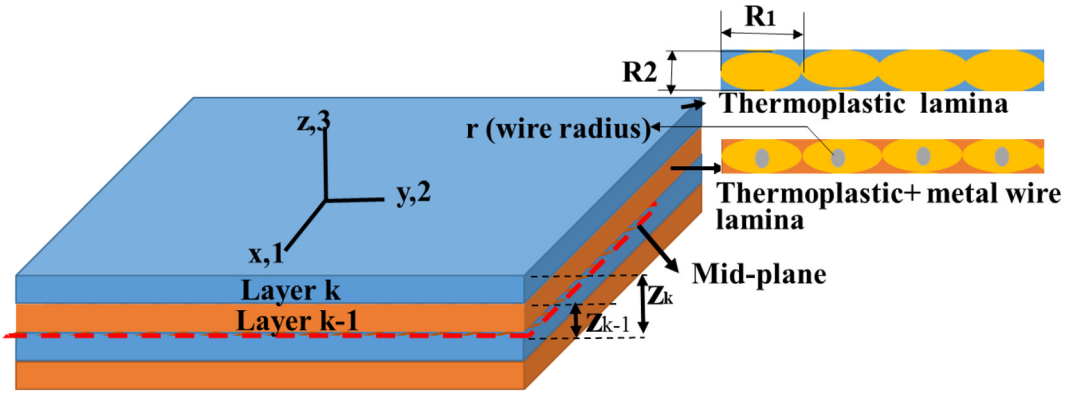

Fig. 5. Schematic of laminated composite structure used in CLPT method.

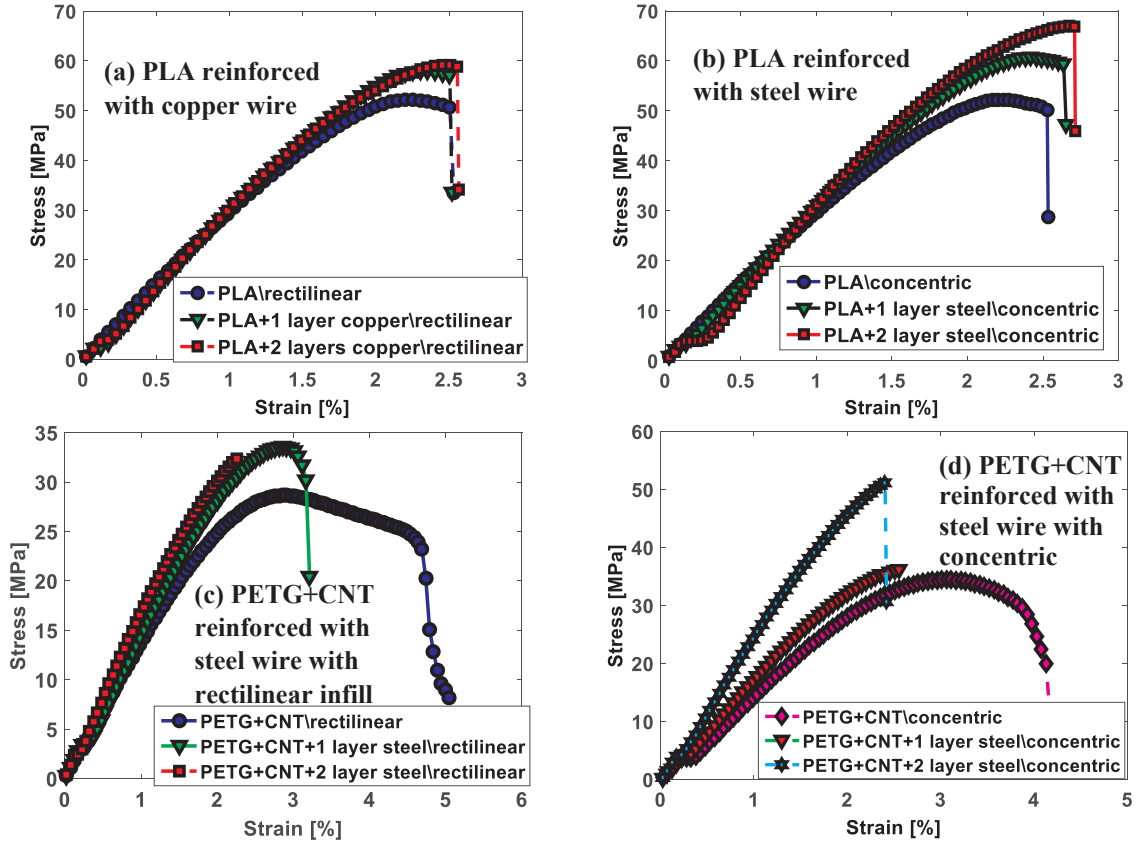

Fig. 6. Tensile test result of 3D printed metal fiber reinforced specimen.

4. Results and discussion

4.1. Tensile test results of metal fiber reinforced thermoplastic

Unidirectional tensile testing was employed to show the enhancement in the strength of the samples by adding metal fibers. Fig. 6 shows the tensile test results of the 3D printed metal reinforced samples (3 samples prepared for each composite).

All the samples are made by continuous fiber 3D printing technique with continuous metal wire drawn from the nozzle starting from the second layer. During the preparation of the PLA samples reinforced with copper wires through concentric pattern, the wires were broken regularly due to the high traction force applied by the nozzle movement and the low strength of the copper wire. However, by changing the pattern to rectilinear and increasing the infill density to 100%, the adhesion between the fiber and matrix improved. Thus, all the samples were 3D printed with 100% infill density. Also, only rectilinear pattern was used for 3D printing samples with copper fiber reinforcement in between PLA layers. The copper wire laid perfectly on the surface of the 3D extruded thermoplastic with less breakage by this pattern because of the weaving arrangement. However, the results in Fig. 6(a) shows that copper wire slightly changed the mechanical properties of the samples. Furthermore, increasing the number of layers from 1 to 2 in copper wire with PLA did not affect the tensile strength notably.

Improvement in mechanical properties was observed in the samples with stainless steel (Fig. 6(b)) as compared to copper wire samples. The tensile test results show that 2 layers of steel wire increased the strength of the PLA sample to 69 MPa. Also, adding each layer of continuous steel fiber can increase the tensile strength with a slight increase in strain. Distinctively, the steel reinforced samples were successfully 3D printed with the PETG + CNT filament by both rectilinear and concentric infill patterns due to the high density and viscosity of the matrix.

Fig. 6(c) & (d) show the strength of the samples were enhanced gradually with inserting the steel wire layers in the specimen for both infill patterns. This means PETG + CNT with 2 steel layers has 51 MPa and PETG + CNT without steel has 28.5 MPa strength. Therefore, the increase in strength is 78%. Though, it is obvious that samples with concentric pattern were stronger due to the alignment of fibers and direction of applied force. Besides, the strain rate of the 3D printed samples with PETG + CNT filament reduced as reinforced layers increased.

The photographs of the failed samples during the tensile test from 12 samples discussed above are presented in Fig. 7. It is observed that in the 3D printed samples, the matrix disruption is the main reason of the failure. As shown in Fig. 7, in PLA samples with steel fibers, the fiber is still connected while the thermoplastic is disconnected, which we considered failure. However, due to the better bonding between the metal fiber and the PETG matrix, they both broke at the same time.

4.2. Comparison of theoretical and experimental elastic properties of continuous metal fiber reinforced thermoplastics

The mathematical models, ROM, Halpin-Tsai and CLPT, were used to predict the elastic properties of PLA and PETG + CNT reinforced samples with concentric infill pattern. Fiber length, fiber orientation and porosity are the most important parameters that affect the mechanical properties in composite. In continuous fiber reinforcement method, fiber length is constant and all the fibers are orientated in the same direction, therefore, the effects of the delamination of the layers and voids are more visible [1]. To determine the extent of the void inclusion (porosity) and load transfer within the 3D printed continuous metal fiber samples, their fractured cross section were examined after the tensile test using scanning electron microscope (SEM). Voids were observed between the thermoplastic layers and also around the wires.

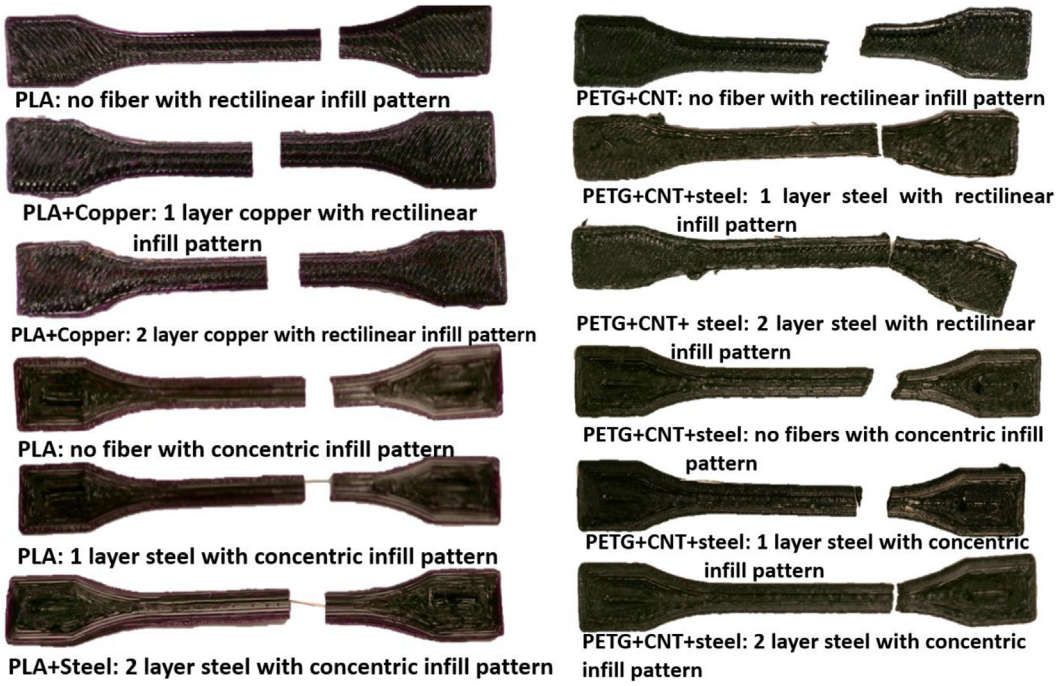

Fig. 7. Failed 3D printed samples after tensile test.

Fig. 8(a) & (b) show the wires were not positioned in the center of the PLA layers and therefore, larger voids formed which extend to the adjacent layer (Fig. 8(a)ii & iii). The porosity of the cross sections shown in Fig. 8(a) is 22% which was determined from image analysis using ImageJ, a Java-based image processing program developed at the National Institutes of Health (NIH) and the Laboratory for Optical and Computational Instrumentation (LOCI). Also Fig. 8(a)i shows that the wires closer to the surface of the specimen pulled out during the tensile test due to the poor interfacial adhesion between the matrix and fiber. However, this can be enhanced by mechanical, chemical,

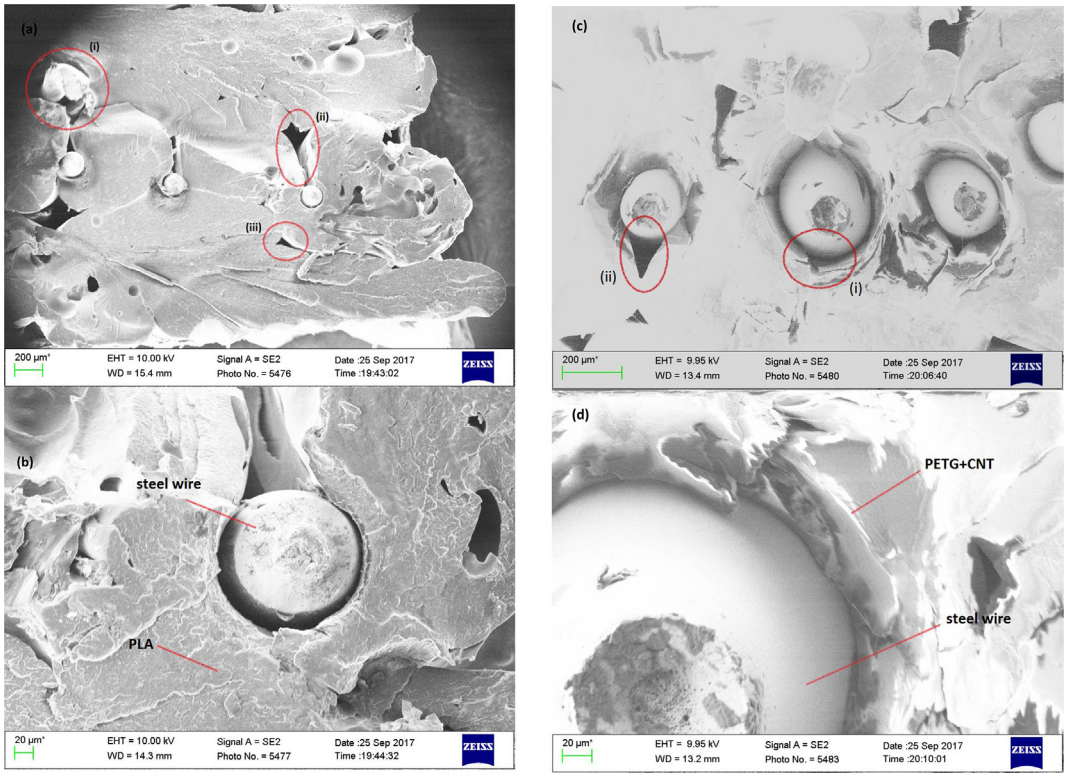

Fig. 8. Scanning electron microscope (SEM) images of samples after tensile test: (a) fractured surface of PLA reinforced with steel wire: (i) steel wire closer to the surface, (ii) void formation between steel wire and PLA layer and (iii) void formation between steel wire and PLA layers, (b) magnified view of PLA and steel showing void formation as well as delamination, (c) fractured surface of PETG + CNT layer with steel wire reinforced: (i) void formation between steel wire and PETG + CNT layers and (ii))void formation between PETG + CNT layers, (d) void formation between PETG + CNT layer and steel wire, magnified view.

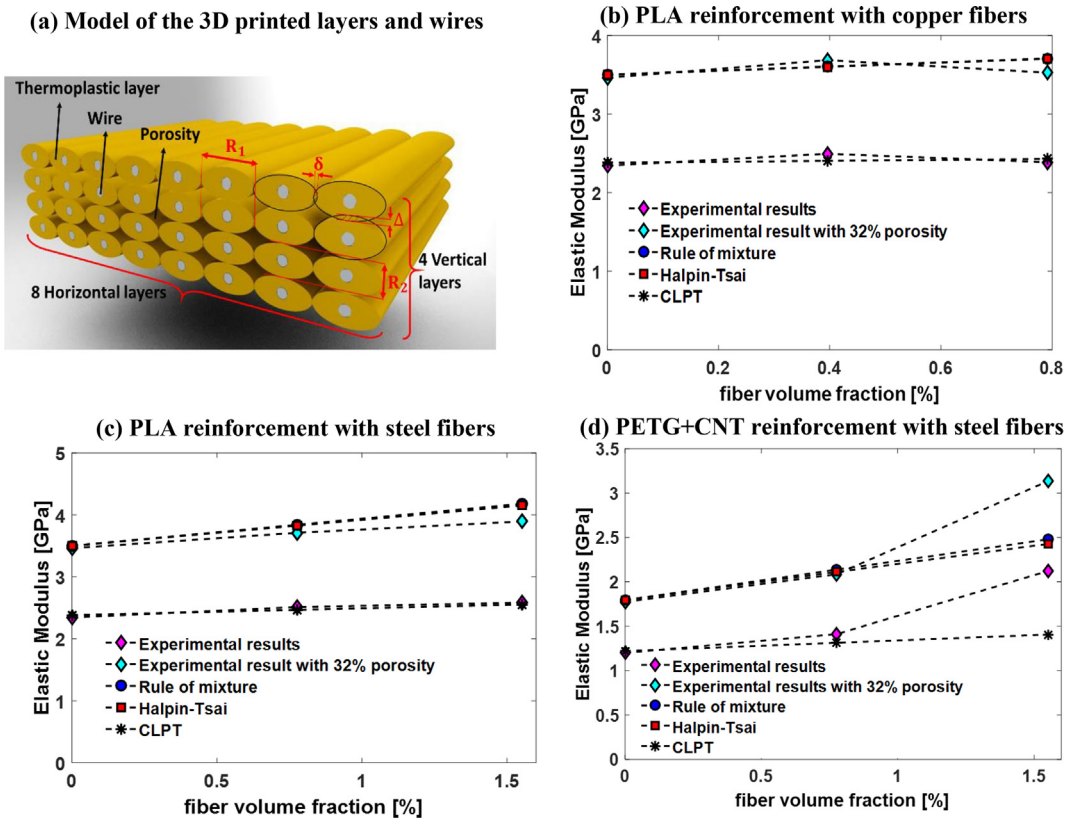

Fig. 9. Comparison of experimental and theoretical tensile strength.

electrochemical and energetic surface treatments of the metal fiber surface as shown in Ref. [45]. On the other hand, the SEM micrographs in Fig. 8(c) & (d), reveal that the steel wires bonded firmly with PETG + CNT layers and less gaps formed between them than PLA layers. The porosity of the cross sections shown in Fig. 8(c) is 20%.

In all samples, the cross-sectional areas of the printed thermoplastic layers were not circular, despite the circular nozzle, because the material were squeezed to the heating bed and other printed composite layers. Thus, the cross section of the thermoplastic layers was assumed as elliptical shape with diameters of 1.61 by 0.8 mm in the modeling section. The total extruded plastic lines on horizontal layer was 8 (similar with the experiment) (Fig. 9(a)). The theoretical models without considering the porosity did not show a good agreement with the experimental data. However, there is a good agreement between the theoretical and experimental results when 32% voids were considered for each sample. This porosity value was calculated by considering the summation of the gap between the elliptical cross section of the lamina. The porosity is calculated based on the elliptical cross-sectional area and flatting effects δ (shown in Fig. 8(a)) and negative gap between the layers Δ(that can be measured experimentally) [46]:

$$Porosity\ \% = 1 - \frac{\pi R_1 R_2}{(2R_1 - \delta)(2R_2 - \Delta)} \tag{17}$$

where R_1 and R_2 are the radii of the elliptical layers (Fig. 9(a)).

The three different models discussed before were used to simulate the elastic modulus and compare with experimental results. All the results for different materials are shown in Fig. 9. For the PLA samples reinforced with copper, increasing the wire layers (fiber volume fraction) did not improve the modulus as it was expected by the theoretical model. This can be due to the copper wires breakage by the extruder traction force. This wire breakage affected the thermoplastic layer alignment and bonding. Therefore, the tensile modulus didn't increase as the number of wire layers increase. Additionally, as SEM images show, steel fibers had a better bonding with PETG + CNT layers than PLA layers. Hence, increasing the wire layers in PETG + CNT sample, decreased the void contents and the difference of the theoretical and experimental results decreases as shown in Fig. 9(c) & (d).

The CLPT inherently consists of porosity in the model, which results in a very good agreement between the experimental and the simulated results except for reinforced PETG + CNT (Fig. 9(d)) that has higher amount of steel. In order to improve the strength further, the porosity can be reduced by increasing the resolution of 3D printer [44].

4.3. Tensile test results of the silicone elastomer

Ecoflex 00-30 was chosen for developing the soft part of the bioinspired joint since it has an adequate young's modulus to overcome the problem of lateral deflections and twisting. Fig. 10(a) & (b) show tensile test results of casted and 3D printed Ecoflex 00-30. All the casted samples had tensile strength of 0.62 ± 0.1 MPa, while the highest strain was 700%. The tensile strength of 3D printed elastomer was lower than the casted ones, while the strain was increased to 800%. These results are comparable with other studies on casted Ecoflex-30 and found 600% strain under 8 MPa stress [47]. This is also the first time that the tensile properties of 3D printed Ecoflex 00-30 was studied and compared to the casted samples. Our tensile test results, elasticity of 800% at a load below 0.4 MPa is a significant, which was due to the addition of silicone thinner.

5. Robotic structure manufacturing with continuous fiber 3D printing technology

It is obvious that smaller tensile modulus is beneficial since it reduces the required force for bending the joints in the desired direction. Therefore, using 3D printer to build the soft parts along with reinforced structures can optimize the structural performance and reduce the manufacturing process time (Fig. 11(a)). The soft material (elastomer) can be used to cover the bone-like structures (joints) in bioinspired

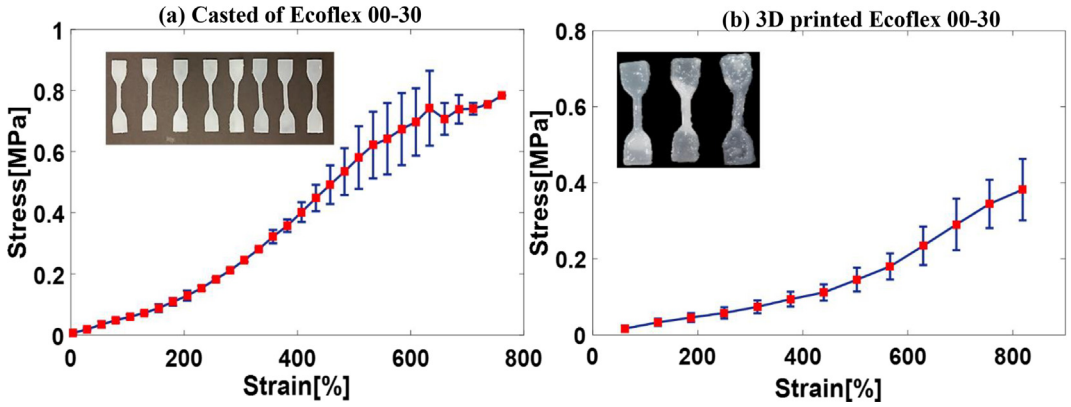

Fig. 10. Tensile test result of Ecoflex 00-30.

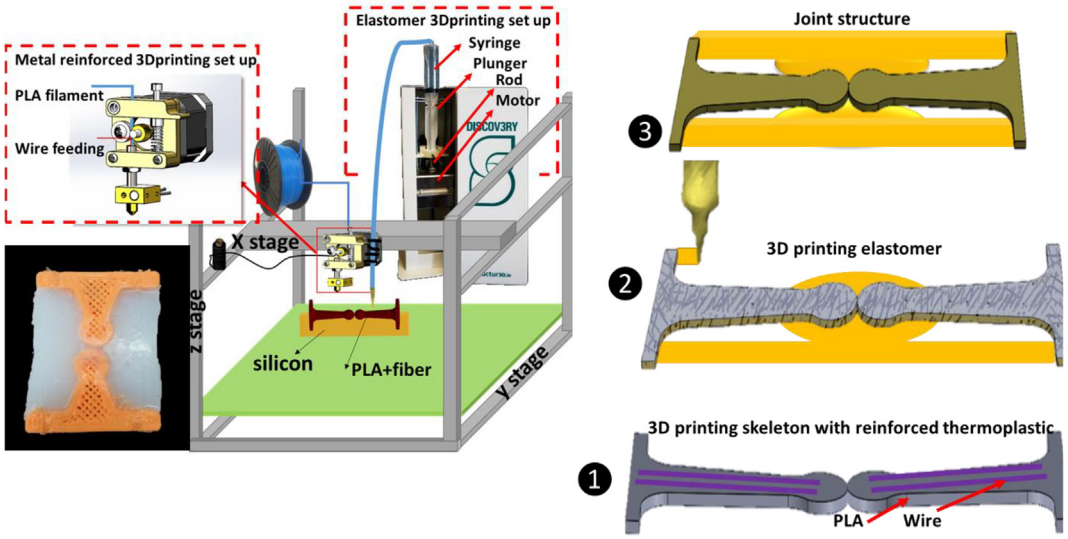

Fig. 11. (a) 3D printer setup for multimaterial 3D printing, (b) fabrication procedure of musculoskeletal joint.

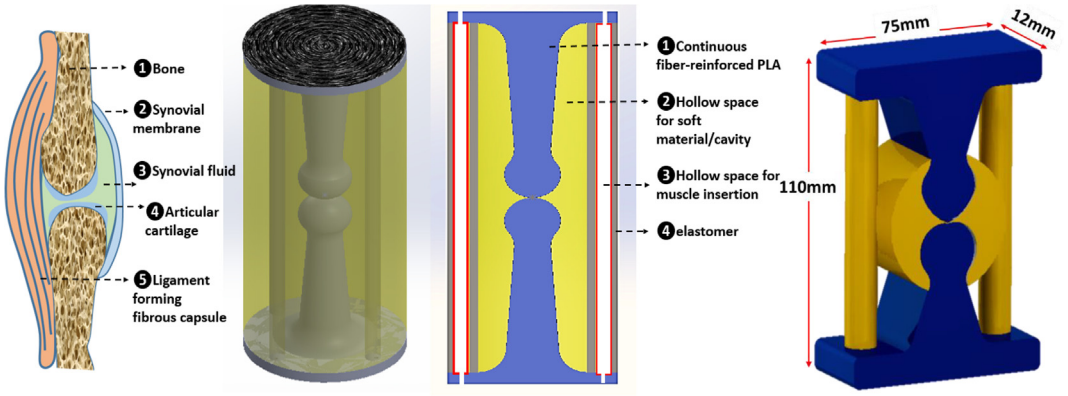

Fig. 12. Joint fiber structure: (a) Structure of a synovial joint, (b) isometric view, (c) sectional view and (d) optimized design for 3D printing.

design of robots (Fig. 11(b)).

A new structure is proposed based on the discussion so far on stronger materials along with soft materials (heterogeneous materials) as shown in Fig. 12, which can be adaptable for 3D printing both large-scale parts and micro level structures with slight modifications. The proposed bioinspired joint consists of a ball-and-socket joint surrounded by silicone to generate multi-dimensional actuation. The reinforced ball and socket joint was 3D printed with PLA reinforced with steel wire. The excess wires that came out of the layers during 3D printing at sharp edges of the bone-like structure (Fig. 13(b)) helped holding the soft silicone attached to the hard PLA parts and create smoother transition between hard and soft parts. This is very important outcome that was observed and should be investigated further in the future. To accommodate multimaterial printing, after the brass nozzle cooled down, the plastic cone nozzle fixed adjacent to it and the elastomeric parts were printed on the same bed. Sample prototype were fabricated as a whole (as one single piece) as shown in Fig. 13(d&f). The structure has capability to bend 180°, Fig. 13(c) with increasing the

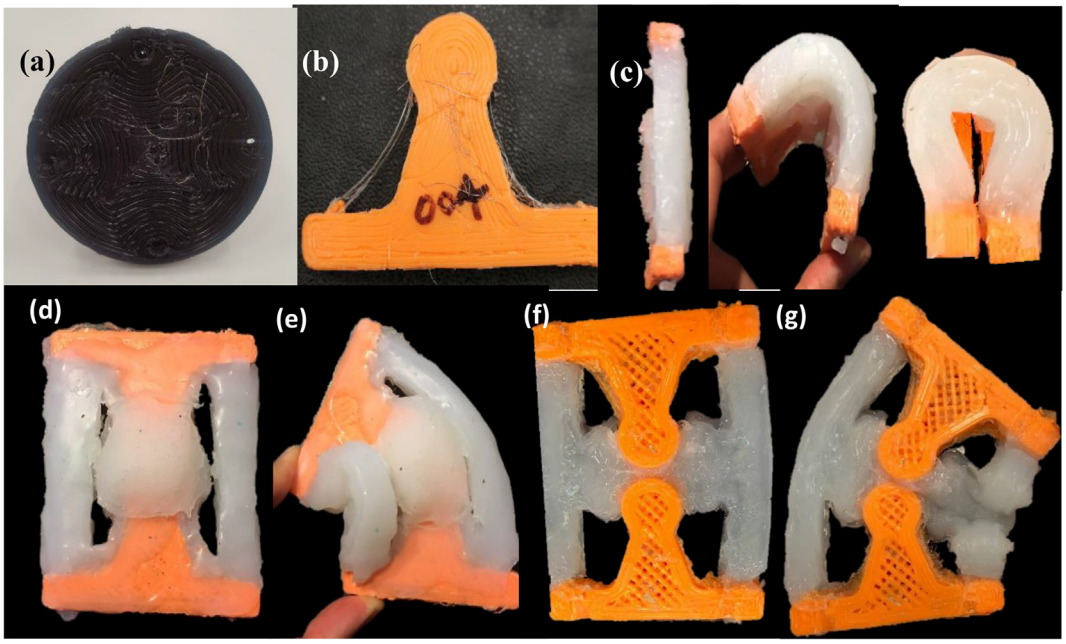

Fig. 13. Structures 3D printed by metal reinforced plastic and soft elastomer method: (a) Circular shape 3D printed with less wire deflection, (b) shapes with sharp angles has more deflection of wire and plastic layers. (c) Side view of the joint structure and flexibility of it to bend 180° from side. (d) 3D printed endoskeleton joint with reinforced PLA and soft Ecoflex 00-30 and cutting the extra silicone and (e) it's bending capability, (f) fully 3D printed joint with silicone elastomer without any post processing fabrication and (g) it's bending capability.

force without any deformation of the PLA 3D printed part, Fig. 13(e & g). The 3D printed elastomer part can even achieve higher dimension accuracy and less thickness compared to the traditional casting method. However, the quality of the structure is affected by the low resolution of the printer for both hard and soft material, which can be further improved in the future.

Future works include creating structures that are more complex by employing a higher resolution nozzle and adding support material that can be 3D printed along with the elastomer. Melted sugar can be considered as a support material with a good adhesion to the elastomer without changing the surface properties [48]. Improvements in the mechanical quality of 3D printed parts, offer the potential to print more complex composite structures, such as reinforced robotic parts. There are few studies available with use of different reinforcement methods for 3D printing a complete structure [19,23]. The further development of these 3 dimensional modeling techniques is expected to be useful for the fabrication of multicomponent structures or devices with multiple applications in microfluidics, robotics, and bionics.

6. Conclusion

The aim of this work was to enhance the mechanical properties of thermoplastics by 3D printing continuous fiber reinforcement along with fabrication of elastomer, all together using a multimaterial 3D printing set up. A new process for simultaneous fabrication of stronger thermoplastic and highly stretchable elastomer materials to produce bioinspired joint was demonstrated. This process has benefits of minimizing process time and material quantities, and reducing waste through additive manufacturing techniques, which are inherently linked to economic and environmental benefits. Currently, multifunctional material manufacturing is one of the greatest challenges and even though several methods have been proposed in this area, they are expensive and haven not been transferred to industry due to scalability [30]. We studied 3D printing of metal reinforced (copper and steel wires) in thermoplastic host materials (PLA, PETG + CNT) for illustration, and compared their mechanical properties with available theoretical models. The efficiency of continuous fiber reinforcement depends on the matrix material and the adhesion between the fiber and matrix because of the voids formation. We demonstrated printing of a bioinspired joint consisting of soft and hard structures, which can be used in robotics. Further, we showed 3D printing of soft elastomer that greatly simplifies the manufacturing of soft robotic joints that can also be beneficial for manufacturing of soft pneumatic actuators. Ultimately, we hope to be able to produce many types of 3D printed bioinspired structures like tendons, cartilage, and skin that mimics soft tissue. Optimizing the structure, improving resolution, fabricating complicated structures, and embedding actuation unit in elastomer are the focus of our next work.

Acknowledgment

The authors would like to acknowledge the support of the Office of Naval Research (ONR), Young Investigator Program, under Grant No. N00014-15-1-2503.

Appendix A. Supplementary data

Supplementary data to this article can be found online at https://doi.org/10.1016/j.compstruct.2018.11.019.

References

[1] van der Klift F, Koga Y, Todoroki A, Ueda M, Hirano Y, Matsuzaki R. 3D printing of continuous carbon fibre reinforced thermo-plastic (CFRTP) tensile test specimens. Open J Compos Mater 2016;6:18–27.
[2] Berman B. 3-D printing: the new industrial revolution. Bus Horiz 2012;55(2):155–62.
[3] Tymrak BM, Kreiger M, Pearce JM. Mechanical properties of components fabricated with open-source 3-D printers under realistic environmental conditions. Mater Des 2014;58:242–6.
[4] Bak D. Rapid prototyping or rapid production? 3D printing processes move industry towards the latter. Assembly Automation 2003;23(4):340–5.
[5] Campbell TA, Ivanova OS. 3D printing of multifunctional nanocomposites. Nano Today 2013;8(2):119–20.
[6] Farahani RD, Dube M, Therriault D. Three-dimensional printing of multifunctional nanocomposites: manufacturing techniques and applications. Adv Mater 2016;28(28):5794–821.
[7] Ning F, Cong W, Hu Z, Huang K. Additive manufacturing of thermoplastic matrix

composites using fused deposition modeling: a comparison of two reinforcements. J Compos Mater 2017. 0021998317692659.
[8] Baumann F, Julian Scholz, Jürgen Fleischer, Investigation of a new approach for additively manufactured continuous fiber-reinforced polymers. In: 1st Cirp conference on composite materials parts manufacturing, cirp-ccmpm2017. 2017: Karlsruhe, Germany. p. 323–328.
[9] Weng ZX, et al. Mechanical and thermal properties of ABS/montmorillonite nanocomposites for fused deposition modeling 3D printing. Mater Des 2016;102:276–83.
[10] Guo SZ, et al. 3D printing of a multifunctional nanocomposite helical liquid sensor. Nanoscale 2015;7(15):6451–6.
[11] Postiglione G, et al. Conductive 3D microstructures by direct 3D printing of polymer/carbon nanotube nanocomposites via liquid deposition modeling. Compos Part a-Appl Sci Manuf 2015;76:110–4.
[12] Sun K, et al. 3D printing of interdigitated Li-ion microbattery architectures. Adv Mater 2013;25(33):4539–43.
[13] Jain SK, Tadesse Y. Fabrication of polylactide/carbon nanopowder filament using melt extrusion and filament characterization for 3D printing. Int J Nanosci 2018.
[14] Potnuru A, Tadesse Y. Investigation of polylactide and carbon nanocomposite filament for 3D printing. Prog Addit Manuf 2018.
[15] Tekinalp HL, et al. Highly oriented carbon fiber-polymer composites via additive manufacturing. Compos Sci Technol 2014;105:144–50.
[16] Zhong WH, et al. Short fiber reinforced composites for fused deposition modeling. Mater Sci Eng a-Struct Mater Properties Microstruct Process 2001;301(2):125–30.
[17] Mori KI, Maeno T, Nakagawa Y. Dieless forming of carbon fibre reinforced plastic parts using 3D printer. In: 11th international conference on technology of plasticity, Ictp 2014, 2014. 81: p. 1595–1600.
[18] Namiki M, Ueda M, Todoroki A, Hirano Y, Matsuzaki R, 3D printing of continuous fibre reinforced plastic. In: Proceedings of the society of the advancement of material and process engineering 2014: Seattle.
[19] Li NY, Li YG, Liu ST. Rapid prototyping of continuous carbon fiber reinforced polylactic acid composites by 3D printing. J Mater Process Technol 2016;238:218–25.
[20] Bettini P, et al. Fused deposition technique for continuous fiber reinforced thermoplastic. J Mater Eng Perform 2017;26(2):843–8.
[21] Dickson AN, Barry JN, McDonnell KA, Dowling DP. Fabrication of Continuous Carbon, Glass and Kevlar fibre reinforced polymer composites using Additive Manufacturing. Addit Manuf 2017;16:146–52.
[22] Tian XY, et al. Recycling and remanufacturing of 3D printed continuous carbon fiber reinforced PLA composites. J Cleaner Prod 2017;142:1609–18.
[23] Yang CC, et al. 3D printing for continuous fiber reinforced thermoplastic composites: mechanism and performance. Rapid Prototyping J 2017;23(1):209–15.
[24] Yao XH, et al. Evaluation of carbon fiber-embedded 3D printed structures for strengthening and structural-health monitoring. Mater Des 2017;114:424–32.
[25] Matsuzaki R, et al. Three-dimensional printing of continuous-fiber composites by in-nozzle impregnation. Sci Rep 2016:6.
[26] Melenka GW, Schofield JS, Dawson MR, Carey JP. Evaluation and prediction of the tensile properties of continuous fiber-reinforced 3D printed structures. Compos Struct 2016;153:866–75.
[27] Parandoush P, et al. Laser assisted additive manufacturing of continuous fiber reinforced thermoplastic composites. Mater Des 2017;131:186–95.
[28] 3DXTech, 3DXNano™ ESD PETG + Carbon Nanotube Filament, in 3DXNano™ ESD, 3DXTech, Editor.
[29] Justo J, et al. Characterization of 3D printed long fibre reinforced composites. Compos Struct 2018;185:537–48.
[30] Ferreira ADBL, Novoa PRO, Marques AT. Multifunctional material systems: a state-of-the-art review. Compos Struct 2016;151:3–35.
[31] Mansouri MR, et al. 3D-printed multimaterial composites tailored for compliancy and strain recovery. Compos Struct 2018;184:11–7.
[32] Zolfagharian A, et al. Evolution of 3D printed soft actuators. Sensors Actuators a-Phys 2016;250:258–72.
[33] Wehner M, et al. An integrated design and fabrication strategy for entirely soft, autonomous robots. Nature 2016;536(7617):451.
[34] Muth JT, et al. Embedded 3D printing of strain sensors within highly stretchable elastomers. Adv Mater 2014;26(36):6307–12.
[35] Hinton TJ, et al. 3D printing PDMS elastomer in a hydrophilic support bath via freeform reversible embedding. ACS Biomater Sci Eng 2016;2(10):1781–6.
[36] Patel DK, et al. Highly stretchable and UV curable elastomers for digital light processing based 3D printing. Adv Mater 2017:29(15).
[37] Tadesse Y, Wu L, Saharan LK. Musculoskeletal system for bio-inspired robotic systems. Mech Eng 2016;138(3):S11.
[38] Pal S. Design of Artificial Human Joints & Organs. Springer; 2014.
[39] Jones RM. Mechanics of Composite Materials. CRC Press; 1998.
[40] Facca AG, Kortschot MT, Yan N. Predicting the elastic modulus of natural fibre reinforced thermoplastics. Compos Part a-Appl Sci Manuf 2006;37(10):1660–71.
[41] Halpin JC, Kardos JL. The Halpin-Tsai equations: a review. Polym Eng Sci 1976;16(5):344–52.
[42] Melenka GW, et al. Evaluation of dimensional accuracy and material properties of the MakerBot 3D desktop printer. Rapid Prototyping J 2015;21(5):618–27.
[43] Gu P, Li L. Fabrication of biomedical prototypes with locally controlled properties using FDM. Cirp Ann-Manuf Technol 2002;51(1):181–4.
[44] Parandoush P, Lin D. A review on additive manufacturing of polymer-fiber composites. Compos Struct 2017;182:36–53.
[45] Molitor P, Barron V, Young T. Surface treatment of titanium for adhesive bonding to polymer composites: a review. Int J Adhes Adhes 2001;21(2):129–36.
[46] Li L, Sun Q, Bellehumeur C, Gu P. Composite modeling and analysis for fabrication of FDM prototypes with locally controlled properties. J Manuf Processes 2002;4(2):129–41.
[47] Case JC, White EL, Kramer RK. Soft material characterization for robotic applications. Soft Rob 2015;2(2):80–7.
[48] Hamidi A, Jain S, Tadesse Y. 3D printing PLA and silicone elastomer structures with sugar solution support material. SPIE Smart Structures and Materials + Nondestructive Evaluation and Health Monitoring. International Society for Optics and Photonics; 2017.